Convective washout reduces the antidiarrheal efficacy of enterocyte surface–targeted antisecretory drugs

Byung-Ju Jin,[1,2] Jay R. Thiagarajah,[1,2,3] and A.S. Verkman[1,2]

[1]Department of Medicine and [2]Department of Physiology, University of California, San Francisco, San Francisco, CA 94143
[3]Department of Pediatrics, Massachusetts General Hospital, Boston, MA 02114

Secretory diarrheas such as cholera are a major cause of morbidity and mortality in developing countries. We previously introduced the concept of antisecretory therapy for diarrhea using chloride channel inhibitors targeting the cystic fibrosis transmembrane conductance regulator channel pore on the extracellular surface of enterocytes. However, a concern with this strategy is that rapid fluid secretion could cause convective drug washout that would limit the efficacy of extracellularly targeted inhibitors. Here, we developed a convection–diffusion model of washout in an anatomically accurate three-dimensional model of human intestine comprising cylindrical crypts and villi secreting fluid into a central lumen. Input parameters included initial lumen flow and inhibitor concentration, inhibitor dissociation constant (K_d), crypt/villus secretion, and inhibitor diffusion. We modeled both membrane-impermeant and permeable inhibitors. The model predicted greatly reduced inhibitor efficacy for high crypt fluid secretion as occurs in cholera. We conclude that the antisecretory efficacy of an orally administered membrane-impermeant, surface-targeted inhibitor requires both (a) high inhibitor affinity (low nanomolar K_d) to obtain sufficiently high luminal inhibitor concentration (>100-fold K_d), and (b) sustained high luminal inhibitor concentration or slow inhibitor dissociation compared with oral administration frequency. Efficacy of a surface-targeted permeable inhibitor delivered from the blood requires high inhibitor permeability and blood concentration (relative to K_d).

INTRODUCTION

Excessive intestinal fluid secretion occurs in enterotoxin-mediated secretory diarrheas caused by *Vibrio cholera* and enterotoxigenic *Escherichia coli* (Field, 1979). The rate-limiting step in fluid secretion is chloride transport from the enterocyte cytoplasm into the intestinal lumen, which creates the electroosmotic force driving sodium and water secretion (Murek et al., 2010; Venkatasubramanian et al., 2010; Thiagarajah and Verkman, 2012). Cell culture and animal models (Chao et al., 1994; Gabriel et al., 1994; Thiagarajah et al., 2004) indicate that elevation in cyclic nucleotides caused by bacterial enterotoxins activates the CFTR, a chloride channel expressed on the luminal surface of enterocytes. CFTR inhibition is thus predicted to be of clinical benefit as antisecretory therapy in diarrheas caused by bacterial enterotoxins (Al-Awqati, 2002; Zhang et al., 2012).

We identified a class of small molecules, the glycine hydrazides and the related malonic acid hydrazides (MalH), as CFTR inhibitors that target the extracellular-facing pore of CFTR (Muanprasat et al., 2004). An extracellular site-of-action was suggested by patch-clamp measurements showing outwardly rectifying whole-cell currents and rapid single-channel flicker (Muanprasat et al., 2004), and proven from CFTR inhibition by membrane-impermeant MalH–polyethylene glycol conjugates (Sonawane et al., 2006). Subsequently, multivalent membrane-impermeant conjugates of MalH with lectins (Sonawane et al., 2007) and polyethylene glycols (Sonawane et al., 2008) were synthesized with K_d < 100 nM for inhibition of CFTR chloride conductance. These membrane-impermeant, nonabsorbable conjugates showed antisecretory efficacy in closed-loop and sucking mouse models of cholera. Membrane-permeable, absorbable glycine hydrazide analogues were also synthesized for potential therapy of polycystic kidney disease, in which cyst growth is CFTR dependent (Yang et al., 2008).

Nonabsorbable CFTR inhibitors are potentially useful for antisecretory therapy because of their minimal systemic exposure. A glycine hydrazide analogue, iOWH032 (de Hostos et al., 2011), with modest CFTR inhibition potency (K_d of ~8 µM), is currently in early-stage clinical trials for cholera therapy. A natural product, crofelemer, which is thought to act by inhibition of CFTR and calcium-activated chloride channels (Tradtrantip et al., 2010), is also in clinical trials (Cottreau et al., 2012). Crofelemer consists of large proanthocyanidin oligomers that are predicted to be membrane impermeable and thus externally acting.

Correspondence to Alan S. Verkman: alan.verkman@ucsf.edu
Abbreviation used in this paper: MalH, malonic acid hydrazides.

The Rockefeller University Press $30.00
J. Gen. Physiol. Vol. 141 No. 2 261–272
www.jgp.org/cgi/doi/10.1085/jgp.201210885

A potentially important though largely ignored concern in the application of externally targeted inhibitors is washout as a result of convection caused by rapid fluid secretion. Convection effects cannot be addressed easily in animal models because of differences from humans in crypt–villus geometry and fluid secretion rates, as well as the lack of suitable animal models of secretory diarrhea. As diagrammed in Fig. 1 A, the intestine contains a dense array of long, narrow cylindrical crypts that secrete fluid into a central lumen. Because of fluid convection, crypt fluid secretion is predicted to reduce inhibitor concentration at the enterocyte surface and hence reduce inhibitor efficacy. Further, if therapeutic inhibitor concentration is not sustained in the intestinal lumen, its antisecretory effect would diminish rapidly unless inhibitor dissociation from its target at the enterocyte surface is slow compared with the time between oral doses. Here, we model CFTR inhibitor washout to predict the conditions (concentration/target affinity, dissociation rate) under which an extracellularly targeted antisecretory drug could be effective in reducing intestinal fluid secretion.

MATERIALS AND METHODS

Model formulation

Fig. 1 A diagrams a cross section of a generic intestinal villus–crypt unit, as found in mid-jejunum, which consists of a long, narrow aqueous compartment bounded by a cylindrical layer of epithelial cells. The crypts project in an outward radial direction from the intestinal wall, and the villi project in an inward radial direction. The inhibitor target, CFTR, is heterogeneously distributed in the lumen-facing (apical) membrane of epithelial cells along the crypt–villus axis, with its extracellular surface exposed to the luminal fluid. Based on published anatomical data in human male adult mid-jejunum (Loehry and Creamer, 1969; Marsh and Swift, 1969; Trbojević-Stanković et al., 2010), typical crypt length is 150 µm and inner diameter (of the aqueous lumen) is 20–25 µm; typical villus length is 350 µm and inter-crypt spacing is ∼100 µm. Volume flux across the epithelium at location z along the crypt–villus, $J_v(z)$, depends on CFTR density, the magnitude of the secretory stimulus, and the concentration of inhibitor contacting the villus–crypt wall. In cholera, typical fluid secretion rate in mid-jejunum is ∼4.5 ml/h per cm intestine (Banwell et al., 1970; Van Loon et al., 1992; Bearcroft et al., 1997), which, together with a crypt density of 12,500 cm^{-2} (Trbojević-Stanković et al., 2010) and a jejunal diameter of 4–5 cm, corresponds to a single-crypt fluid secretion rate of $\sim 4 \times 10^{-7}$ cm^3/min ($\sim 7 \times 10^{-2}$ $\mu L/cm^2/s$ at the crypt surface). Fluid viscosity in the crypt lumen is ∼10-fold greater than that of water, as measured by photobleaching and dye polarization (Naftalin et al., 1995). Material properties and baseline parameters are listed in Table 1. For a single cylindrical crypt–villus unit, the computed parameters include inhibitor concentration C_i (r,z) and velocity V_i (r,z), in which cylindrical symmetry allows specification of location by radial dimension r and axial position z.

Fig. 1 B shows the generic three-dimensional geometry of the intestine, with crypts and villi projecting radially from the cylindrical intestinal wall. The diameter of the intestinal lumen is orders of magnitude greater than crypt length. Fluid entering the intestinal lumen has a specified inhibitor concentration and flow velocity, which may vary in time (because of intermittent oral administration). Because the intestinal lumen is cylindrically symmetric and large compared with crypt dimensions, diffusion–convection for the geometry shown in Fig. 1 B can be simplified to that of a truncated radial wedge of fluid with

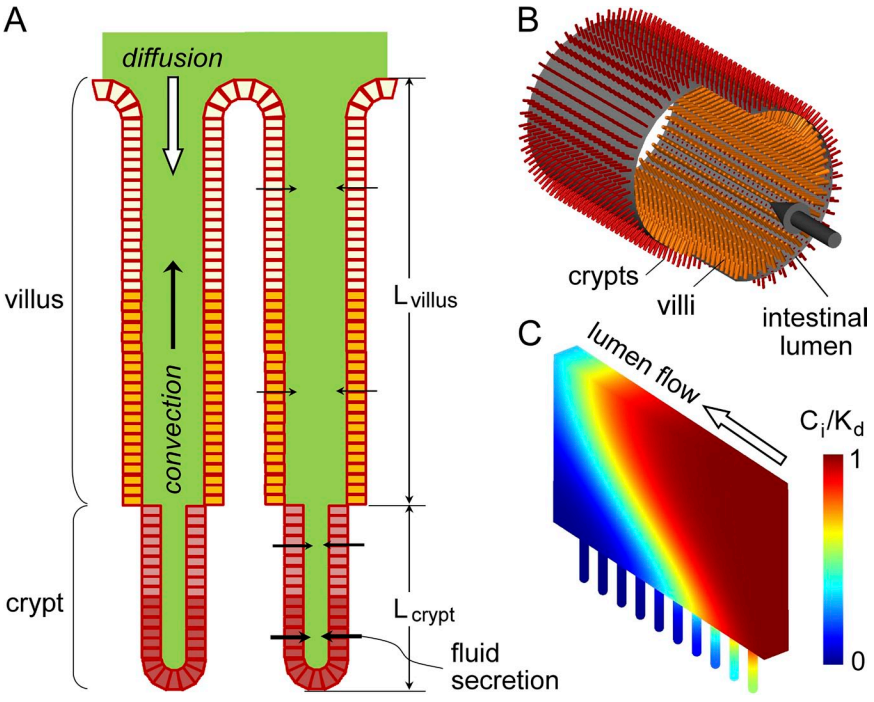

Figure 1. Model of drug convection–diffusion in intestinal crypt–villus units. (A) Schematic of epithelial cell–lined crypt–villus units (lengths, L_{crypt} and L_{villus}). Fluid secretion into the lumen produces convective (upward) solute transport. (B) Three-dimensional model of radially oriented crypt–villus units projecting from a cylindrical lumen. (C) Section near the intestinal wall showing crypt–villus units and a wedge of luminal aqueous-phase volume. Cylindrical symmetry reduces computation complexity. An example of pseudocolored inhibitor concentration profile is shown.

attached crypt–villus units as diagrammed in Fig. 1 C, as described in Results.

List of parameters

Parameters for single-crypt/villus computations:

D, diffusion coefficient in crypt/villus lumen (cm^2/s)
$J_v(z)$, volume flux across the epithelium at location z along the crypt ($\mu L/cm^2/s$)
$J_v^o(z)$, volume flux across the epithelium in the absence of inhibitor ($\mu L/cm^2/s$)
ΣJ_v, total volume flux from crypt ($\mu L/s/crypt$)
$C_i(r,z)$, inhibitor concentration at location r,z (μM)
$V_i(r,z)$, vectorial flow velocity at location r,z (cm/s)
$P_i(r,z)$, pressure at location r,z (Pa)
ΔP, pressure difference between $P_i(r,z)$ and reference pressure in the intestine (Pa)
C_o, inhibitor concentration at outer boundary (μM)
$J_b(z)$, transepithelial volume flux of (permeable) inhibitor ($mol/cm^2/s$)
$J_b^o(z)$, initial transepithelial volume flux of inhibitor ($mol/cm^2/s$)
P_{inh}, transepithelial inhibitor permeability (cm/s)
C_b, inhibitor concentration in blood (μM)
K_d, inhibitor–CFTR binding dissociation constant (μM)
k_1, dissociation rate constant (min^{-1})
k_1, association rate constant ($\mu M^{-1}\ min^{-1}$)
ρ, fluid density (kg/m^3)
η, fluid dynamic viscosity ($Pa \cdot s$)
Δt, computation time step (s)
L, crypt length (μm)
d, crypt diameter (μm)
$f_b(z)$, occupied fraction of inhibitor binding site

Additional parameters for multi-crypt/villus computations:

D_L, diffusion coefficient in the intestinal lumen (cm^2/s)
D_M, diffusion coefficient in the mucosa (crypt/villus region) (cm^2/s)
η_L, fluid dynamic viscosity in the lumen ($Pa \cdot s$)
η_M, fluid dynamic viscosity in the mucosa ($Pa \cdot s$)
L_V, villus length (μm)
L_C, crypt length (μm)
d_V, villus diameter (μm)
d_C, crypt diameter (μm)
d_L, intestinal lumen diameter (μm)
U(x,y,z), inhibitor velocity in the intestinal lumen (cm/s)
U_{mean}, mean inhibitor velocity in the lumen (cm/s)
s, distance from the center of the lumen (cm)
s_o, distance from the center of the lumen to the top of the villus (cm)

Model computations

Models of convection–diffusion in single crypt–villus units (two-dimensional) and the full intestine (three-dimensional) were implemented using COMSOL Multiphysics (version 3.4; COMSOL). The model is specified by a diffusion equation describing inhibitor convection–diffusion coupled with the Navier–Stokes equation describing the fluid flow field. The convection–diffusion equation is

$$\frac{\partial C_i}{\partial t} = \underbrace{-V_i \cdot \nabla C_i}_{\text{convection}} + \underbrace{D\nabla^2 C_i}_{\text{diffusion}}, \quad (1)$$

which contains convection and diffusion terms. The velocity field, V_i, in the convection term was computed from the Navier–Stokes equation for an incompressible fluid and the continuity equation,

$$\rho \frac{\partial V_i}{\partial t} + \rho (V_i \cdot \nabla) V_i = -\nabla P_i + \eta \nabla^2 V_i \quad (2)$$

$$\nabla \cdot V_i = 0, \quad (3)$$

where ρ is fluid density, P_i is pressure, and η is dynamic viscosity.

For computations on single-crypt/villus units, as shown in Fig. 2 A, constant inhibitor concentration was imposed at the outer boundary and an insulation boundary condition (no flux through membrane) was imposed at the crypt/villus surface. Volume flux at the crypt surface in the steady state, $J_v(z)$, depends on volume flux in the absence of inhibitor, $J_v^o(z)$, and local inhibitor concentration, $C_i(r_o,z)$,

$$J_v(z) = J_v^o(z) / [1 + C_i(r_o, z) / K_d], \quad (4)$$

where K_d is the equilibrium dissociation constant for inhibitor-target (CFTR) binding.

To model a membrane-permeable inhibitor in which inhibitor is transported from the circulation into the crypt/villus lumen, the transepithelial flux of inhibitor, $J_b(z)$, is described by

$$J_b(z) = P_{inh} \cdot [C_b - C_i(r,z)] = J_b^o(z) \cdot [1 - C_i(r_o,z) / C_b], \quad (5)$$

where P_{inh} describes inhibitor permeability across the intestinal epithelium, and C_b is inhibitor concentration in blood. A convective flux boundary condition was imposed at the outer boundary and at the crypt/villus surface.

In multi-crypt computations, the same flux boundary condition is imposed at the crypt surface. The parabolic velocity profile at the lumen inlet was calculated from mean lumen velocity as

$$U(x,y,z) = 2U_{mean} \cdot [1 - (s / s_o)^2], \quad (6)$$

where s_o is the distance from the lumen center to the top of villi, and s is the distance from the center of the lumen. Symmetric boundary conditions are imposed at the two side walls and a slip boundary condition at the top surface. Details on boundary conditions are provided in the Appendix (Figs. A1 and A2, and Table 2).

The computation time to obtain the steady-state solution was ~10 min for single-crypt computations and 4–24 h for multi-crypt computations, as performed on an HP Z600 workstation (Xeon E5645 CPU and 32G RAM; Intel). The time step was automatically computed in COMSOL Multiphysics from mesh size and property value variation. Computation validation studies are provided in the supplemental text.

Inhibition of net fluid secretion was computed as the ratio of total crypt–villus fluid secretion in the presence versus absence of inhibitor,

$$\%\ \text{inhibition} = 100 \cdot (1 - \sum J_v / \sum J_v^o). \quad (7)$$

For modeling the kinetics of inhibitor washout, the fraction of bound inhibitor, f_b (0 to 1, $f_b = C_i/(C_i + K_d)$ in the steady state), is described by the differential equation,

$$df_b(z)/dt = k_1 \cdot [1 - f_b(z)] \cdot C_i - k_{-1} \cdot f_b(z), \quad (8)$$

where k_{-1} is inhibitor dissociation rate constant, and k_1 is inhibitor bimolecular association rate constant, subject to the condition, $K_d = k_{-1}/k_1$.

The percent inhibition of fluid secretion along the length of the intestine was deduced from the computational results done for small segments, in which inhibitor concentration in each segment is diluted progressively because of fluid secretion. Conservation of inhibitor molecules (Eq. 9) and of fluid volume (Eq. 10) requires

$$U_{out} C_{out} = U_{in} C_{in} \quad (9)$$

$$U_{out} \cdot A_L = U_{in} \cdot A_L + \sum J_v \cdot (\pi d_L / w), \quad (10)$$

where C_{in} and C_{out} are inhibitor concentration at the inlet and the outlet in each segment, U_{in} and U_{out} are mean lumen velocity, A_L is luminal cross-sectional area, d_L is lumen diameter, w is segment length, and $\sum J_v$ (equal to $\sum J_v^o$ [1 − 0.01 · % inhibition]) is total single-segment secretion rate. Percent inhibition at each segment was specified by an empirical fit of computed results at the segment.

Total percent inhibition (over the length of the intestine) is the ratio of integrated secreted fluid without versus with inhibitor. Total secreted fluid in the absence of inhibitor was computed by summation of flux from each segment,

$$\text{Secreted fluid (no inhibitor)} = \sum J_v^o \cdot (\pi d_L / w) \cdot (L_{int} / \Delta x), \quad (11)$$

where $\sum J_v^o$ is initial single-segment secretion rate, d_L is lumen diameter, w is segment length, L_{int} intestinal length, and Δx is segment length. Total secreted fluid in the presence of inhibitor was computed from the difference in luminal flow in the final segment without versus with inhibitor, so that percent inhibition becomes

$$\text{total \% inhibition} = 100 \cdot [1 - (U_{out}^N - U_{in}^1) A_L / \{\sum J_v^o \cdot (\pi d_L / w) \cdot (L_{int} / \Delta x)\}], \quad (12)$$

where U_{out}^N is mean flow velocity in the final segment, and U_{in}^1 is mean inlet flow velocity at the first segment, where U_{out}^N is calculated iteratively applying conservation conditions (Eqs. 9 and 10).

Online supplemental material

The online supplemental material includes additional information on the mathematical modeling, including the validations of computation time and the number of mesh elements, and details of the secretion ratio (J_v^o) calculation. It is available at http://www.jgp.org/cgi/content/full/jgp.201210885/DC1.

RESULTS

Single crypt–villus computations for a membrane-impermeant, surface-targeted inhibitor

We first analyzed convection–diffusion for a single crypt–villus unit to explore the main features of the model.

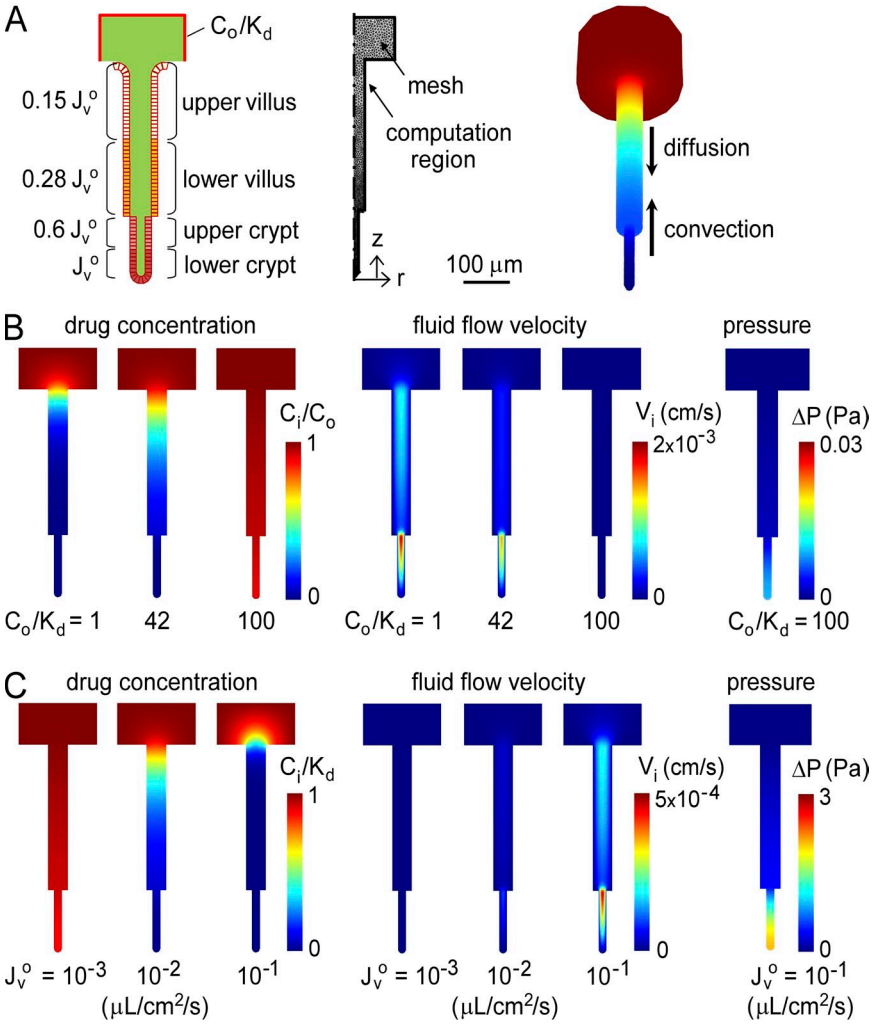

Figure 2. Convective inhibitor washout in single crypts. Inhibitor convection–diffusion was solved for a cylindrical crypt–villus unit exposed at its outer boundary (intestinal lumen) to a constant concentration of membrane-impermeant inhibitor, C_o/K_d. (A) Cross section of a cylindrical crypt–villus unit showing relative J_v^o at indicated regions (left). Two-dimensional computation volume showing mesh elements (middle). Equivalent three-dimensional crypt–villus unit showing downward inhibitor diffusion and upward convection. (B) Steady-state profiles of drug concentration (left), fluid flow velocity (middle), and pressure (right) for single-crypt diffusion–convection for indicated C_o/K_d, with $J_v^o = 4 \times 10^{-2}$ μL/cm²/s. (C) Steady-state profiles for indicated J_v^o, with $C_o/K_d = 1$.

Fig. 2 A (left) shows a cross section of the crypt–villus structure in mid-jejunum (where the majority of fluid secretion occurs in cholera), which consists of a 350-μm-long villus shown aligned with a 150-μm-long crypt. Based on reported data on CFTR distribution (Jakab et al., 2011), relative $\sum J_v(r_o,z)$ in the absence of inhibitor was taken as 1.0 (lower 50% of crypt), 0.6 (upper 50% of crypt), 0.28 (lower 50% of villus), and 0.15 (upper 50% of villus). Fig. 2 A (middle) shows mesh element in the two-dimensional computation region, which, by symmetry, solves the equivalent three-dimensional crypt–villus problem (Fig. 2 A, right).

For the two-dimensional computations, the intervillous region was modeled as a simple cylinder approximating the actual three-dimensional geometry, which is modeled below. We note that the further simplification of our model to one dimension is not possible because of the need to impose unrealistic boundary conditions, which necessitated the inclusion of a "buffer zone" at the crypt–villus outlet in the single-crypt computations. As fluid leaves the crypt–villus unit it takes with it solute and so produces a complex two-dimensional profile extending from the outlet that can be quite large for high flow velocities as found in diarrhea.

Fig. 2 B shows steady-state profiles of drug concentration (left) and fluid flow velocity (middle) for different (dimensionless) C_o/K_d, in which C_o/K_d is fixed at the outer computational region. The increase in pressure is negligible, as shown in the right panel of Fig. 2 B for $C_o/K_d = 100$. Convective effects are observed in the profiles, with marked axial concentration and velocity gradients. At fixed fluid secretion rate (in the absence of inhibitor) of $J_v^o = 4 \times 10^{-2}$ μL/cm^2/s, increasing C_o/K_d to 100 allowed inhibitor access deep in crypts (Fig. 2 B, left). Increased inhibitor concentration reduced fluid velocity. Fig. 2 C shows the steady-state drug concentration and fluid flow velocity profiles at fixed C_o/K_d of 1 for different J_v^o, and the pressure profile for $J_v^o = 10^{-1}$ μL/cm^2/s. Increasing J_v^o reduced inhibitor concentration in crypt-villus units because of convection, with a very small pressure increase of <2 Pa (compared with atmospheric pressure of 10^5 Pa).

Results from computations as in Fig. 2 are summarized in Fig. 3. Fig. 3 A shows the percent inhibition of secreted fluid for the crypt–villus geometry of the mid-jejunum, as deduced from volume flux exiting the crypt without inhibitor versus with inhibitor. The percent inhibition of fluid secretion increased from 0 to 100% with increasing C_o/K_d, as expected, although the apparent IC_{50} for inhibition was substantially increased with increasing J_v^o. For low, near static flow ($J_v^o = 10^{-3}$ μL/cm^2/s), C_o/K_d of 1 produced ∼50% inhibition of fluid secretion, as expected. For J_v^o of 7×10^{-2} μL/cm^2/s, which is typical of cholera, inhibition of net fluid secretion by 50% required C_o/K_d of ∼200, and clinically relevant inhibition by 90% required C_o/K_d of ∼750. Fig. 3 B shows similar computations for the colon, which consists of long, narrow crypts (length 430 μm, diameter 16 μm) without villi. A similar dependence of percent inhibition of fluid secretion on C_o/K_d and J_v^o was seen, in which 50% inhibition of fluid secretion required C_o/K_d of ∼40 for $J_v^o = 7 \times 10^{-3}$ μL/cm^2/s, typical of cholera in colon.

Single crypt/villus computations for a membrane-permeable, surface-targeted inhibitor

Computations were also done for a membrane-permeable, surface-targeted CFTR inhibitor in which the inhibitor enters the crypt–villus lumen from the blood compartment rather than the intestinal lumen. We assume constant inhibitor concentration in blood, with entry into the crypt–villus lumen determined by the (blood-to-lumen) inhibitor concentration gradient and enterocyte permeability.

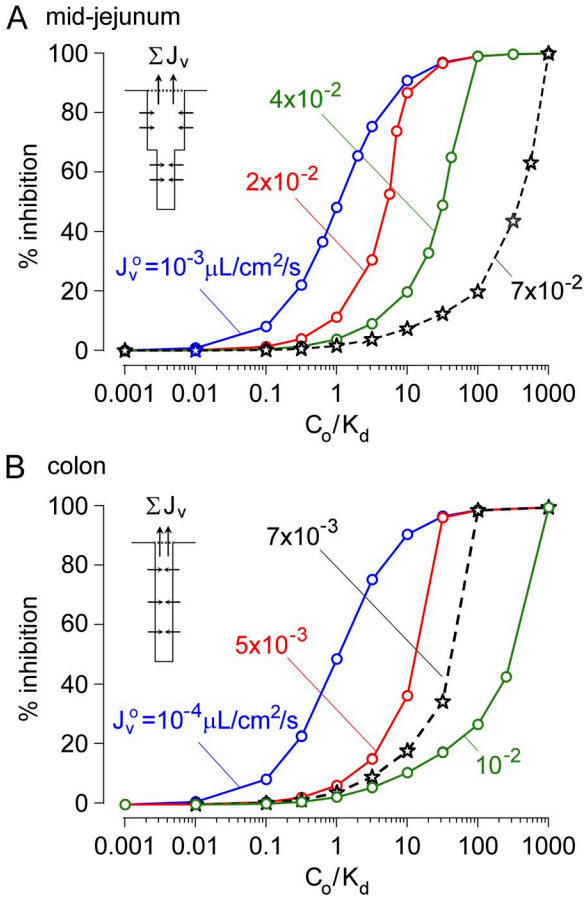

Figure 3. Convective inhibitor washout requires a very high concentration of a membrane-impermeant inhibitor in the intestinal lumen for antisecretory efficacy. (A) Computations done for human mid-jejunal anatomy as in Fig. 2. Percent inhibition of net secreted fluid as a function of C_o/K_d for indicated J_v^o. J_v^o of ∼7×10^{-2} μL/cm^2/s is typical in cholera. (B) Computations done for human colonic anatomy with long, narrow crypts without villi. Percent inhibition of net secreted fluid as a function of C_o/K_d for indicated J_v^o. J_v^o of ∼7×10^{-3} μL/cm^2/s in colon is typical in cholera.

The hypothesis is that high blood inhibitor concentration and enterocyte permeability are required for antisecretory efficacy of a membrane-permeant, externally targeted inhibitor. Our reasoning, as diagrammed in Fig. 4 A, is that inhibitor molecules crossing the enterocyte barrier are convected away from the luminal surface, impairing their ability to inhibit CFTR.

Fig. 4 B shows drug concentration profiles for different drug permeability coefficients for transepithelial transport from blood into the crypt–villus lumen, P_{inh} (left), and for different fluid secretion rates, J_v^o. Convective washout of luminal inhibitor is seen as reduced C_i/C_b with increasing J_v^o. Fig. 4 C summarizes the percent inhibition of net secreted fluid as a function of P_{inh} for different J_v^o at fixed C_b = 10 µM and K_d = 10 µM. At a low J_v^o of 10^{-3} µL/cm^2/s, half-maximal inhibition required P_{inh} of ∼10^{-7} cm/s, whereas at high J_v^o of 7 × 10^{-2} µL/cm^2/s, typical of cholera, 50% of maximal inhibition required an ∼100-fold increased P_{inh} of ∼10^{-5} cm/s. Maximal inhibition was 50% for $C_b = K_d$, as expected. Similar computations are shown in Fig. 4 D for C_b = 1 µM and K_d = 0.1 µM, where maximal inhibition is ∼100%. At low J_v^o of 10^{-3} µL/cm^2/s, half-maximal inhibition required P_{inh} of ∼10^{-9} cm/s, whereas at higher J_v^o of 7 × 10^{-2} µL/cm^2/s, half-maximal inhibition required P_{inh} of ∼5 × 10^{-6} cm/s. These computations show that convective washout effects can occur for a membrane-permeable, surface-targeted inhibitor.

Multi-crypt computations with three-dimensional intestinal geometry

Computations were also done for the three-dimensional intestine as diagrammed in Fig. 1 B. Our approach was to first analyze percent inhibition versus C_o/K_d (as done in Fig. 3 A for single crypt–villus units) for a short segment of intestine (mid-jejunum), and then extend the computation to model many meters of intestine. Fig. 5 A shows an en face view of the crypt–villus geometry in this model, as deduced from electron microscopy data (Loehry and Creamer, 1969; Marsh and Swift, 1969). Finger-shaped villi of 100–250-µm diameter extend out of the plane, with inter-crypt distance of ∼100 µm and a crypt to villus ratio of ∼3. We modeled crypts and villi as cylinders with semispherical outer surfaces. Villus length was taken as 350 µm, with an outer diameter of 120 µm and inter-villus spacing of 150 µm. Crypt length was taken as 150 µm, with an inner diameter of 20 µm and inter-crypt distance of 100 µm. The villi to crypt ratio was 3, giving a crypt density of 13,333 cm^{-2}, similar to the measured value of 12,500 cm^{-2} (Trbojević-Stanković et al., 2010). Fig. 6 A (middle) shows a small segment of 1-mm length and 150-µm width used as the computational volume (chosen to allow a crypt to villus ratio of 3). The computational volume is composed of two layers, mucosa and lumen, of different viscosities. Fig. 5 A (right) shows 80,000–150,000 mesh elements in the computation volume.

Fig. 5 B shows the steady-state profiles of drug concentration. Similar to the profiles in Fig. 2 B, increasing

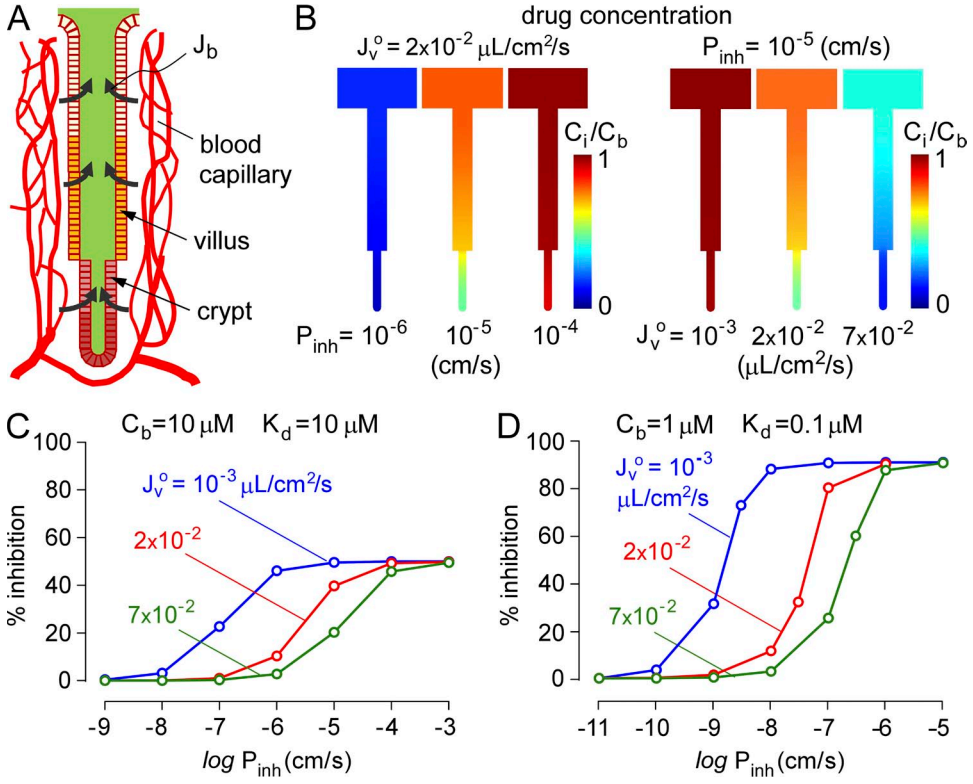

Figure 4. Model of antidiarrheal efficacy of a membrane-permeant inhibitor. Computations done for human mid-jejunal crypt–villus anatomy. (A) Schematic showing inhibitor permeation across enterocytes from blood into the crypt–villus lumen, which depends on inhibitor transepithelial permeability coefficient, P_{inh}, and blood concentration C_b. (B) Steady-state inhibitor concentration profiles for indicated P_{inh} for J_v^o = 2 × 10^{-2} µL/cm^2/s (left), and for indicated J_v^o for P_{inh} = 10^{-5} cm/s (right), both for C_b = 10 µM and K_d = 10 µM. (C) Percent inhibition of net secreted fluid as a function of P_{inh} for indicated J_v^o at C_b = 10 µM and K_d = 10 µM. (D) Same as in C, with C_b = 1 µM and K_d = 0.1 µM.

J_v^o produced greater convection, reducing inhibitor access deep in crypts. Fig. 5 C shows percent net fluid inhibition versus C_o/K_d for different J_v^o, analogous to the single crypt–villus analysis in Fig. 3 C. C_o/K_d was ~1 for low J_v^o, as expected, increasing substantially for higher J_v^o. These computations for three-dimensional crypt–villus geometry support the robustness of the conclusion that greatly increased C_o/K_d is needed for effective inhibition at high fluid secretion rates.

The short segment of intestinal surface with anatomically accurate three-dimensional geometry was extended to model the human mid-jejunum with 5-mm length and 5-cm diameter (Fig. 5 D, top). Assuming a well-mixed intestinal lumen beyond the level of villus tips, the steady-state profile of fluid inhibition along the intestine was computed as described under Model computations in Materials and methods. Fig. 5 D (bottom) shows percent inhibition along the intestine for different initial lumen axial flow velocities, U_{mean}, representing different axial starting points along the length of the intestine. The percent inhibition decreases along the length of intestine as inhibitor is diluted by secreted fluid from crypts and villi.

Fig. 5 E shows deduced percent inhibition versus C_o/K_d plots for different U_{mean} for J_v^o of 7×10^{-2} μL/cm^2/s, typical of cholera. Because of inhibitor dilution effects, the percent inhibition versus C_o/K_d profiles is right-shifted, indicating the requirement of high C_o/K_d (>1,000) for efficient reduction in intestinal fluid secretion. Even greater C_o/K_d would be predicted without the assumption of a well-mixed intestinal lumen.

Inhibitor washout kinetics limits antidiarrheal efficacy

The computations described above for an orally administered (membrane-impermeable) inhibitor were done for the steady state, with constant inhibitor concentration entering the intestinal lumen (at the boundary of the computation region). However, because of intermittent oral administration, inhibitor concentration varies over time, with little inhibitor present in the intestinal lumen much of the time. To model inhibitor washout, inhibitor concentration in the lumen was reduced at time 0 from C_o/K_d to 0 (step-function). Fig. 6 A shows the kinetics of inhibitor washout for a single crypt–villus unit for dissociation rate constant, $k_{-1} = 10^{-1}$ min^{-1}.

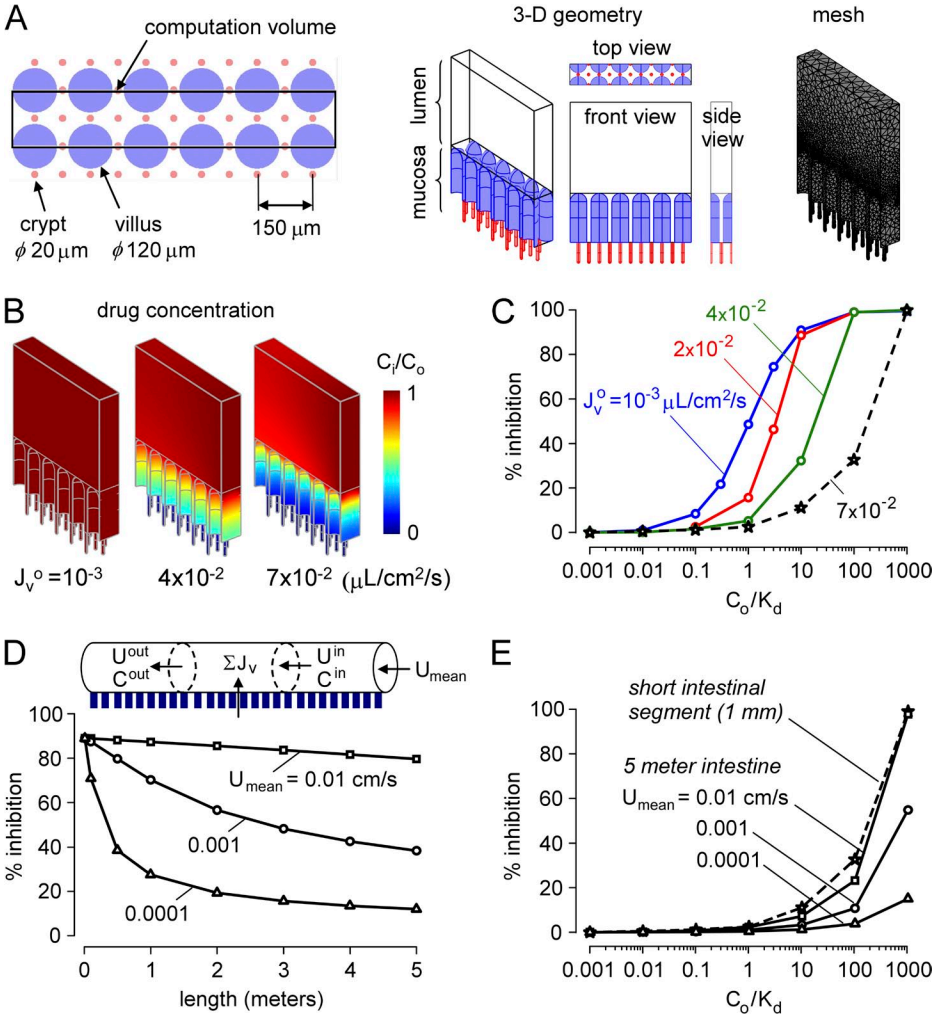

Figure 5. Inhibitor washout in a three-dimensional multi-crypt model of the intestine. (A) Crypt–villus geometry in the three-dimensional model showing a matrix of spatially distinct narrow crypts and relatively wide villi. (B) Drug concentration profiles for steady-state solution of multi-crypt diffusion–convection for indicated J_v^o for C_o/K_d = 10. (C) Percent inhibition of net secreted fluid as a function of C_o/K_d for indicated J_v^o. J_v^o of ~7×10^{-2} μL/cm^2/s is typical in cholera. (D) Percent inhibition along the intestine for indicated lumen axial mean velocity, U_{mean}. Segmental percent inhibition in C was described by an empirical regression to the equation: % inhibition = $\alpha \cdot \exp[\beta \cdot \log_{10}(C_{in}/K_d)]$, with α = 3.523 and β = 1.112 for $J_v^o = 7 \times 10^{-2}$ μL/cm^2/s, typical of cholera. (E) Percent inhibition for 5-m-long intestinal segment as a function of C_o/K_d for indicated U_{mean}. Results for a short (1-mm) intestinal segment are shown for comparison.

Washout occurs over time as CFTR inhibitor dissociation releases inhibitor molecules that are convected out of the crypt. In addition to crypt–villus geometry, the determinants of washout kinetics include k_{-1}, fluid secretion rate, and C_o/K_d. Fig. 6 B shows the kinetics of loss of inhibition of fluid secretion for mid-jejunum, with parameters chosen to give ~90% inhibition of fluid secretion before washout. For a k_{-1} of 10^{-1} min^{-1} (well below that expected for small-molecule inhibitors with micromolar K_d) and a high C_o/K_d of 10, washout occurs in tens of minutes. Very low k_{-1} is required to greatly slow inhibitor washout. For the three-dimensional crypt–villus geometry, predicted washout is even more rapid, occurring over a few minutes for a k_{-1} of 10^{-1} min^{-1} (Fig. 6 C).

DISCUSSION

CFTR offers a unique target for antisecretory therapy of enterotoxin-mediated diarrheas because it is expressed on the luminal membrane of enterocytes and is hence exposed to the aqueous-phase contents of the intestinal lumen. The luminal exposure of CFTR allows the possibility of developing inhibitors that are targeted to its external surface that could act after oral administration and without systemic absorption. High throughput screening of chemically diverse small-molecule libraries identified glycine hydrazides and related analogues that blocked the external CFTR pore directly (Muanprasat et al., 2004). The glycine hydrazides were engineered into nonabsorbable macromolecular conjugates with high affinity binding to CFTR and slow dissociation (Sonawane et al., 2007, 2008). However, because of the high volume of fluid that can be secreted in diarrhea, inhibitor washout from the surface of the intestine is a concern. Convection–diffusion, as fluid is secreted out of the long, narrow intestinal crypts, is predicted to reduce inhibitor concentration at the luminal surface of the crypt epithelial cells. Washout effects can also be important for systemically absorbed inhibitors that target an extracellular site on crypt epithelial cells, as inhibitor dissociation from the surface and subsequent convection out of crypts can reduce surface inhibitor concentration. Although orally administered nonabsorbable drugs are in use (Charmot, 2012), such as cholesterol-binding resins and antimicrobials, drug targeting to the external site of a luminal receptor on the intestinal epithelium is a new concept in drug delivery. Because there was no precedent for existing drugs using this targeting strategy, or data to evaluate the magnitude or kinetics of washout effects, we modeled the CFTR–inhibitor system in the intestine using data applicable to secretory diarrhea, although our model would apply in general to drugs that target luminal receptors on enterocytes.

Qualitatively, the effects of convection and diffusion on washout can be derived from a simple dimensional analysis of the convection and diffusion terms in Eq. 1, giving a single dimensionless parameter, the Peclet number (Pe),

$$\text{washout effect (Pe)} = \frac{\text{convection term}}{\text{diffusion term}} \approx \frac{V_i \cdot \nabla C_i}{D\nabla^2 C_i} \approx \frac{V_i \frac{C_i}{L}}{D\frac{C_i}{L^2}} = \frac{V_i L}{D} \approx 4\frac{L^2 J_v^o}{dD},$$

where V_i is flow velocity, L is length of crypt or villus, D is diffusion coefficient, J_v^o is initial volume flux, and d is crypt/villus diameter. The washout effect is proportional to crypt or villus length and volume flux, and

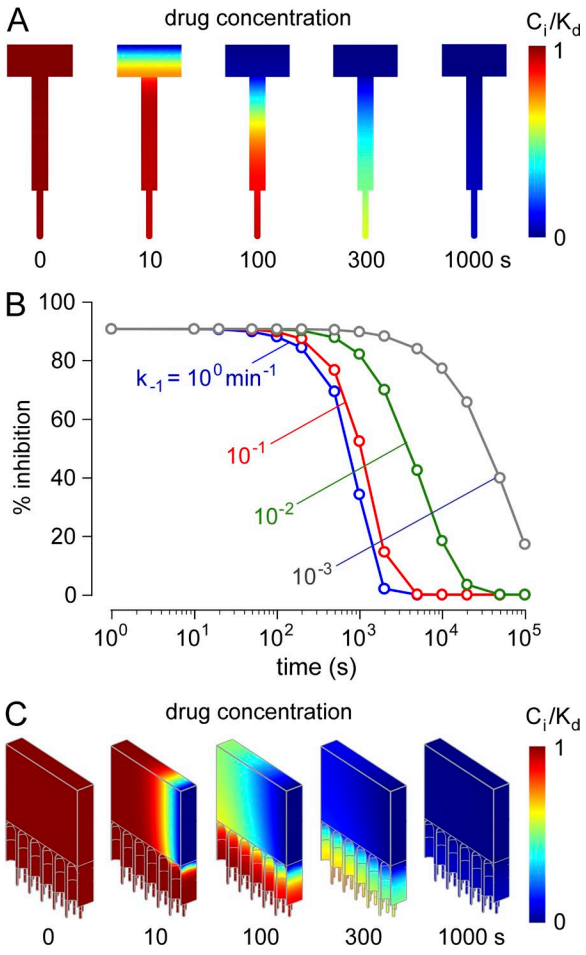

Figure 6. Rapid washout of a luminally delivered membrane-impermeant inhibitor. After steady-state inhibition, inhibitor concentration in the intestinal lumen was reduced from C_o/K_d to 0. (A) Drug concentrations profiles for kinetic (presteady-state) solution of single-crypt diffusion–convection for $C_o/K_d = 10$, $J_v^o = 10^{-3}$ μL/cm^2/s, and $k_{-1} = 10^{-1}$ min^{-1}. (B) Kinetics of inhibition of fluid secretion after inhibitor washout. Percent inhibition of net fluid secretion as a function of time after washout for $C_o/K_d = 10$, $J_v^o = 10^{-3}$ μL/cm^2/s, and indicated k_{-1}. (C) Washout kinetics for the three-dimensional multi-crypt model for same parameters as in A.

TABLE 1

Material properties and baseline parameters

Material property	Baseline parameter
ρ	Fluid density = 10^3 (kg/m^3)
D_L	Diffusion coefficient in the intestinal lumen = 2×10^{-9} (m^2/s)
D_M	Diffusion coefficient in the mucosa (crypt/villus region) = 2×10^{-10} (m^2/s)
η_L	Fluid dynamic viscosity in the lumen = 10^{-3} (Pa · s)
η_M	Fluid dynamic viscosity in the mucosa = 10^{-2} (Pa · s)
L_V	Villus length = 350 (μm)
L_C	Crypt length = 150 (μm)
d_V	Villus diameter = 120 (μm)
d_C	Crypt diameter = 20 (μm)
d_L	Intestinal lumen diameter = 5 (cm)

inversely proportional to crypt or villus radius and diffusion coefficient. Substantial washout effect occurs for small crypt/villi radius and long crypt/villi length. The geometric term (L^2/d) for villi (L = 350 μm, d = 120 μm from effective diameter) is similar to that for crypts (L = 150 μm, d = 20 μm), which gives a Pe of ∼14 and 16, respectively, for the severe diarrhea case ($J_v^o = 7 \times 10^{-2}$ μL/cm^2/s). Therefore, both crypts and villi are important determinants of washout, although the washout effect in crypts is greater because of higher fluid secretion rate. In any case, quantitative analysis required full computational analysis because of nonlinear effects and the complex geometry of crypt–villus units.

The main conclusion of the modeling is that the antisecretory efficacy of a surface-targeted channel inhibitor requires both (a) very high luminal inhibitor concentration compared with its K_d, and (b) sustained very high luminal inhibitor concentration or slow inhibitor dissociation compared with the interval between oral dosing. For a crypt secretion rate of 7×10^{-2} μL/cm^2/s, typical of cholera, the luminal concentration of a membrane-impermeant inhibitor should be >200 × K_d to reduce net fluid secretion by 50% and 800 × K_d to reduce fluid secretion by 90% (Figs. 3 A and 5 C). Even higher inhibitor concentration is needed if the inhibitor diffusion coefficient is lower than that used in the model here, which may be the case because of mucus and other viscous substances in the aqueous-phase fluid. Further, even if adequate inhibitor concentration in the intestinal lumen is achieved for antisecretory efficacy, a high concentration must be sustained, as delivery of inhibitor-free fluid at the luminal surface results in rapid loss of inhibitor efficacy unless inhibitor dissociation from its luminal target is very slow. For a typical small molecule with low micromolar K_d, dissociation occurs over a few seconds or less, producing significant loss of antisecretory efficacy over minutes (Fig. 6). For oral administration of an inhibitor every few hours, the lumen is exposed to cyclical changes in inhibitor concentration, with little inhibitor present most of the time. Sustained release or other formulations, although potentially helpful, are unlikely to produce sustained therapeutic inhibitor concentrations when the fluid secretion rate is high as in cholera and traveler's diarrhea.

Of the available externally targeted CFTR inhibitors, GlyH-101 (Sonawane et al., 2006) and small-molecule analogues such as MalH (Sonawane et al., 2007) and iOWH032 (de Hostos et al., 2011) have IC_{50} in the range of 2–8 μM and dissociate from CFTR within seconds. We conclude from the modeling here that such compounds would not fulfill criteria (a) or (b). MalH-lectin conjugates have higher affinity (K_d of ∼50 nM) and slow washout over several hours or longer (Sonawane et al., 2007), as the lectin moiety is bound tightly and trapped in the dense glycocalyx lining the intestinal surface. However, although MalH-lectin conjugates can thus fulfill criteria (a) and (b), lectin conjugates may not be practical for antisecretory therapy in developing countries because the lectin moiety significantly increases the drug cost and reduces its stability during storage.

The antidiarrheal efficacy of a surface-targeted, membrane-permeable inhibitor that is systemically absorbed and enters the intestinal lumen from the blood side was also considered. Fluid convection can cause washout of inhibitor molecules that enter the crypt lumen from the blood. Typical intestinal transepithelial permeability coefficients for absorbable drugs, based on Caco-2 data, are in the range of 10^{-6} to 10^{-5} cm/s, with values up to 7×10^{-5} cm/s for the most highly permeable drugs (Usansky and Sinko, 2005). The computations in Fig. 4 indicate that antidiarrheal efficacy is limited by inhibitor convective washout at high drug $K_d \sim C_b$ for typical drug permeability ($10^{-6} \sim 10^{-5}$ cm/s). A more potent drug (K_d of ∼0.1 C_b) predicted good antidiarrheal efficacy. Therefore, provided that therapeutic drug concentration in the blood can be maintained, and that drug K_d is sufficiently low and drug permeability sufficiently high, a surface-targeted, membrane-permeable inhibitor can be efficacious in secretory diarrhea.

Although our model was formulated to closely recapitulate the in vivo three-dimensional geometry of a high density of radially oriented crypt–villus units lining

the intestinal lumen, several features of the intestine were not included in the model. The model does not consider differences in the detailed geometry and transport properties of the different regions of the small and large intestine, nor does it include fluid absorption or mechanical peristalsis. Although these additional complexities were not modeled explicitly, the major conclusions of our model are robust and should not be influenced by these fine details. The majority of secreted fluid comes from the jejunum, as was modeled here, and fluid secretion in secretory diarrheas such as cholera greatly exceeds absorption. Peristaltic effects would be predicted to have little time-averaged effect on inhibitor diffusion in the unstirred crypt luminal compartment.

Notwithstanding these potential limitations of our model, we conclude that washout in secretory diarrhea is a major factor for nonabsorbable drugs that target surface receptors or transporters on enterocytes in intestinal crypts. Therapeutic efficacy requires sustained high drug concentration in the intestinal lumen. For the inhibitor–CFTR system, surface-targeted small molecules with micromolar K_d are unlikely to be efficacious for therapy of secretory diarrhea, whereas macromolecular conjugates with nanomolar K_d and very slow dissociation might be effective. We conclude, therefore, that although surface-targeted glycine hydrazide and MalH originally appeared to be attractive candidates for antisecretory therapy, absorbable CFTR inhibitors, such as thiazolidinones (Thiagarajah et al., 2004) and PPQ/BPO compounds (Tradtrantip et al., 2009; Snyder et al., 2011), are better development candidates for CFTR inhibition therapy of enterotoxin-mediated secretory diarrheas.

APPENDIX

Boundary conditions

As described in Materials and methods, the three-dimensional multi-crypt computation involves solution of the diffusion–convection equation for inhibitor concentration and the (incompressible fluid) Navier–Stokes equation for the fluid field. Fig. A1 and Table 2 provide details on boundary conditions.

Lumen inlet boundary condition

The circular lumen inlet has parabolic velocity profile with mean velocity, U_{mean}. Because the intestinal lumen (~5-cm diameter) is much bigger than crypt dimensions (20-μm diameter and 150-μm length), the computation was simplified to greatly reduce computation time. A small segment near the mucosa (crypt and villus), with computation volume of 1,250 μm (crypt length of 150 μm, villus length of 350 μm), was used (Fig. 1 C). The velocity profile at the lumen inlet was taken as part of the parabolic profile as shown in Fig. A2. The lumen inlet boundary condition (the magnitude of mean velocity) had negligible effect on percent inhibition (not depicted) because the viscosity in the mucosa is >10-fold greater than that in the intestinal lumen, so that the flow field produced by secretion is dominant in the crypt/villus mucosa. A constant inhibitor concentration boundary condition was used for the inhibitor concentration at the lumen inlet.

Left and right surface boundary condition

As shown in Fig. 5 A, the small segment containing crypts and villi unit is repeated symmetrically around the lumen, producing laminar flow in the lumen (viscous forces dominant over inertia), $R_e = U_{mean}d_L/(\nu) < 0.1$, where d_L is lumen diameter and ν is kinematic viscosity. Thus, symmetric boundary conditions were imposed at the left and the right surface boundaries.

Top surface boundary condition

A slip boundary condition was used for the Navier–Stokes equation, and an insulation (no flux) boundary condition was used for the diffusion–convection equation.

Crypt and villus surface boundary condition

As described in Materials and methods, the rate of fluid secretion at the crypt and villus surface was determined by initial secretion rate and inhibitor concentration. For a membrane-impermeant inhibitor insulation

TABLE 2

Boundary conditions for Navier–Stokes and diffusion–convection equations

Navier–Stokes equation		Diffusion–convection equation	
(1) Inlet BC (lumen flow velocity)	$U = 2U_{mean} \cdot [1-(s/s_o)^2]$ $V_i = -U \cdot \mathbf{n}$	(1) Inlet BC (constant C_o)	$C = C_o$
(2) Symmetric BC	$\mathbf{n} \cdot V_i = 0$, $\mathbf{t} \cdot [-p\mathbf{I} + \mu(\nabla V_i + (\nabla V_i)^T] = 0$	(2) Symmetric BC	$\mathbf{n} \cdot n = 0$, $N = -D \cdot \nabla C + CV_i$
(3) Slip BC	$\mathbf{n} \cdot V_i = 0$, $\mathbf{t} \cdot [-p\mathbf{I} + \mu(\nabla V_i + (\nabla V_i)^T] = 0$	(3) Insulation BC	$\mathbf{n} \cdot n = 0$, $N = -D \cdot \nabla C + CV_i$
(4) Flux BC	$V_i = -J_v \cdot \mathbf{n}$, $J_v = J_v^o(1 - C_i/(C_i + K_d))$	(4) Insulation BC	$\mathbf{n} \cdot n = 0$, $N = -D \cdot \nabla C + CV_i$
(5) Outlet BC (no viscous stress)	$[\mu(\nabla V_i + (\nabla V_i)^T]\mathbf{n} = 0$, $p = p_0$	(5) Outlet BC (convective flux)	$\mathbf{n} \cdot (-D\nabla C) = 0$

BC, boundary condition; **n**, surface normal vector; **I**, unit vector; ∇, gradient operator. Other variables are defined in the main text.

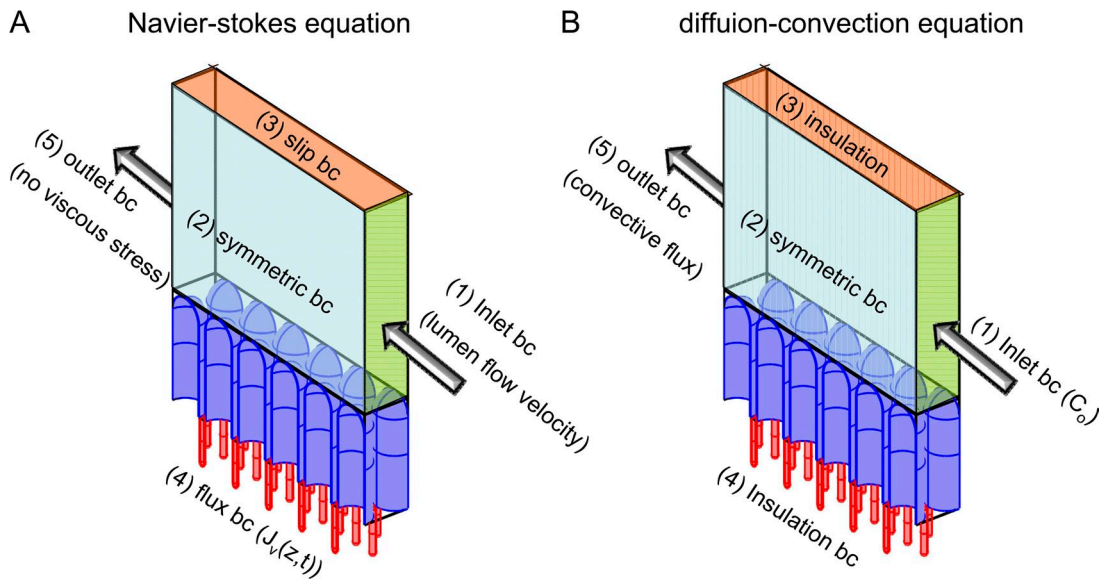

Figure A1. Schematic of boundary conditions for the three-dimensional multi-crypt computation. (A) Boundary conditions for the Navier–Stokes equation. (B) Boundary conditions for the diffusion–convection equation.

(no flux), boundary conditions were imposed at the crypt and villus surfaces.

Lumen outlet boundary condition

Because the lumen outlet is open, a no-viscous stress and pressure boundary condition was used for the Navier–Stokes equation, and a convective flux boundary condition was used for the diffusion–convection equation.

This work was supported by National Institutes of Health grants DK72517, EB00415, HL73856, DK35124, and EY13574.

Edward N. Pugh Jr. served as editor.

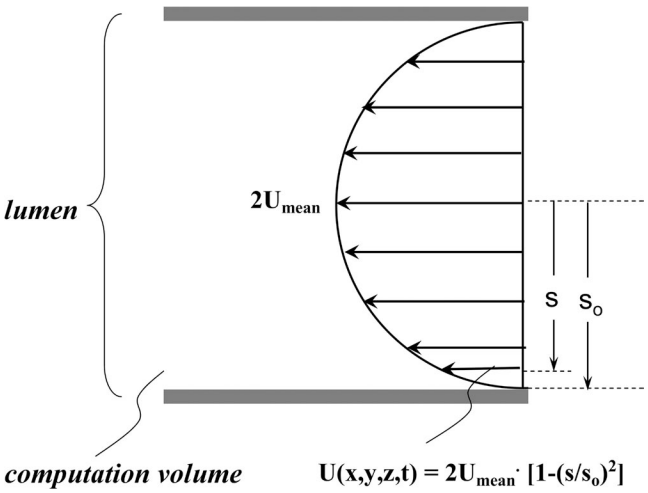

Figure A2. Schematic of inlet boundary condition, where s is distance from the center of the lumen, s_o is distance from the center of the lumen to the top of the villus, and U_{mean} is the mean inhibitor velocity in the lumen.

Submitted: 23 August 2012
Accepted: 3 January 2013

REFERENCES

Al-Awqati, Q. 2002. Alternative treatment for secretory diarrhea revealed in a new class of CFTR inhibitors. *J. Clin. Invest.* 110: 1599–1601.

Banwell, J.G., N.F. Pierce, R.C. Mitra, K.L. Brigham, G.J. Caranasos, R.I. Keimowitz, D.S. Fedson, J. Thomas, S.L. Gorbach, R.B. Sack, and A. Mondal. 1970. Intestinal fluid and electrolyte transport in human cholera. *J. Clin. Invest.* 49:183–195. http://dx.doi.org/10.1172/JCI106217

Bearcroft, C.P., E.A. André, and M.J. Farthing. 1997. In vivo effects of the 5-HT3 antagonist alosetron on basal and cholera toxin-induced secretion in the human jejunum: a segmental perfusion study. *Aliment. Pharmacol. Ther.* 11:1109–1114. http://dx.doi.org/10.1046/j.1365-2036.1997.d01-1389.x

Chao, A.C., F.J. de Sauvage, Y.J. Dong, J.A. Wagner, D.V. Goeddel, and P. Gardner. 1994. Activation of intestinal CFTR Cl^- channel by heat-stable enterotoxin and guanylin via cAMP-dependent protein kinase. *EMBO J.* 13:1065–1072.

Charmot, D. 2012. Non-systemic drugs: a critical review. *Curr. Pharm. Des.* 18:1434–1445.

Cottreau, J., A. Tucker, R. Crutchley, and K.W. Garey. 2012. Crofelemer for the treatment of secretory diarrhea. *Expert Rev. Gastroenterol. Hepatol.* 6:17–23. http://dx.doi.org/10.1586/egh.11.87

de Hostos, E.L., R.K. Choy, and T. Nguyen. 2011. Developing novel antisecretory drugs to treat infectious diarrhea. *Future Med Chem.* 3:1317–1325. http://dx.doi.org/10.4155/fmc.11.87

Field, M. 1979. Mechanisms of action of cholera and Escherichia coli enterotoxins. *Am. J. Clin. Nutr.* 32:189–196.

Gabriel, S.E., K.N. Brigman, B.H. Koller, R.C. Boucher, and M.J. Stutts. 1994. Cystic fibrosis heterozygote resistance to cholera toxin in the cystic fibrosis mouse model. *Science.* 266:107–109. http://dx.doi.org/10.1126/science.7524148

Jakab, R.L., A.M. Collaco, and N.A. Ameen. 2011. Physiological relevance of cell-specific distribution patterns of CFTR, NKCC1, NBCe1, and NHE3 along the crypt-villus axis in the intestine. *Am.*

J. Physiol. Gastrointest. Liver Physiol. 300:G82–G98. http://dx.doi.org/10.1152/ajpgi.00245.2010

Loehry, C.A., and B. Creamer. 1969. Three-dimensional structure of the human small intestinal mucosa in health and disease. *Gut.* 10:6–12. http://dx.doi.org/10.1136/gut.10.1.6

Marsh, M.N., and J.A. Swift. 1969. A study of the small intestinal mucosa using the scanning electron microscope. *Gut.* 10:940–949. http://dx.doi.org/10.1136/gut.10.11.940

Muanprasat, C., N.D. Sonawane, D. Salinas, A. Taddei, L.J. Galietta, and A.S. Verkman. 2004. Discovery of glycine hydrazide pore-occluding CFTR inhibitors: Mechanism, structure–activity analysis, and in vivo efficacy. *J. Gen. Physiol.* 124:125–137. http://dx.doi.org/10.1085/jgp.200409059

Murek, M., S. Kopic, and J. Geibel. 2010. Evidence for intestinal chloride secretion. *Exp. Physiol.* 95:471–478. http://dx.doi.org/10.1113/expphysiol.2009.049445

Naftalin, R.J., P.S. Zammit, and K.C. Pedley. 1995. Concentration polarization of fluorescent dyes in rat descending colonic crypts: evidence of crypt fluid absorption. *J. Physiol.* 487:479–495.

Snyder, D.S., L. Tradtrantip, C. Yao, M.J. Kurth, and A.S. Verkman. 2011. Potent, metabolically stable benzopyrimido-pyrrolo-oxazinedione (BPO) CFTR inhibitors for polycystic kidney disease. *J. Med. Chem.* 54:5468–5477. http://dx.doi.org/10.1021/jm200505e

Sonawane, N.D., J. Hu, C. Muanprasat, and A.S. Verkman. 2006. Luminally active, nonabsorbable CFTR inhibitors as potential therapy to reduce intestinal fluid loss in cholera. *FASEB J.* 20: 130–132.

Sonawane, N.D., D. Zhao, O. Zegarra-Moran, L.J. Galietta, and A.S. Verkman. 2007. Lectin conjugates as potent, nonabsorbable CFTR inhibitors for reducing intestinal fluid secretion in cholera. *Gastroenterology.* 132:1234–1244. http://dx.doi.org/10.1053/j.gastro.2007.02.018

Sonawane, N.D., D. Zhao, O. Zegarra-Moran, L.J. Galietta, and A.S. Verkman. 2008. Nanomolar CFTR inhibition by pore-occluding divalent polyethylene glycol-malonic acid hydrazides. *Chem. Biol.* 15:718–728. http://dx.doi.org/10.1016/j.chembiol.2008.05.015

Thiagarajah, J.R., and A.S. Verkman. 2012. CFTR inhibitors for treating diarrheal disease. *Clin. Pharmacol. Ther.* 92:287–290. http://dx.doi.org/10.1038/clpt.2012.114

Thiagarajah, J.R., T. Broadbent, E. Hsieh, and A.S. Verkman. 2004. Prevention of toxin-induced intestinal ion and fluid secretion by a small-molecule CFTR inhibitor. *Gastroenterology.* 126:511–519. http://dx.doi.org/10.1053/j.gastro.2003.11.005

Tradtrantip, L., N.D. Sonawane, W. Namkung, and A.S. Verkman. 2009. Nanomolar potency pyrimido-pyrrolo-quinoxalinedione CFTR inhibitor reduces cyst size in a polycystic kidney disease model. *J. Med. Chem.* 52:6447–6455. http://dx.doi.org/10.1021/jm9009873

Tradtrantip, L., W. Namkung, and A.S. Verkman. 2010. Crofelemer, an antisecretory antidiarrheal proanthocyanidin oligomer extracted from Croton lechleri, targets two distinct intestinal chloride channels. *Mol. Pharmacol.* 77:69–78. http://dx.doi.org/10.1124/mol.109.061051

Trbojević-Stanković, J.B., N.M. Milićević, D.P. Milosević, N. Despotović, M. Davidović, P. Erceg, B. Bojić, D. Bojić, P. Svorcan, M. Protić, et al. 2010. Morphometric study of healthy jejunal and ileal mucosa in adult and aged subjects. *Histol. Histopathol.* 25:153–158.

Usansky, H.H., and P.J. Sinko. 2005. Estimating human drug oral absorption kinetics from Caco-2 permeability using an absorption-disposition model: model development and evaluation and derivation of analytical solutions for k_a and F_a. *J. Pharmacol. Exp. Ther.* 314:391–399. http://dx.doi.org/10.1124/jpet.104.076182

Van Loon, F.P., G.H. Rabbani, K. Bukhave, and J. Rask-Madsen. 1992. Indomethacin decreases jejunal fluid secretion in addition to luminal release of prostaglandin E2 in patients with acute cholera. *Gut.* 33:643–645. http://dx.doi.org/10.1136/gut.33.5.643

Venkatasubramanian, J., M. Ao, and M.C. Rao. 2010. Ion transport in the small intestine. *Curr. Opin. Gastroenterol.* 26:123–128. http://dx.doi.org/10.1097/MOG.0b013e3283358a45

Yang, B., N.D. Sonawane, D. Zhao, S. Somlo, and A.S. Verkman. 2008. Small-molecule CFTR inhibitors slow cyst growth in polycystic kidney disease. *J. Am. Soc. Nephrol.* 19:1300–1310. http://dx.doi.org/10.1681/ASN.2007070828

Zhang, W., N. Fujii, and A.P. Naren. 2012. Recent advances and new perspectives in targeting CFTR for therapy of cystic fibrosis and enterotoxin-induced secretory diarrheas. *Future Med Chem.* 4:329–345. http://dx.doi.org/10.4155/fmc.12.1